C-terminal tagging, transmembrane domain hydrophobicity, and an ER retention motif influence the secretory trafficking of the inner nuclear membrane protein emerin

Jessica Mella[1], Regan Volk[1], Balyn Zaro[1,2], and Abigail Buchwalter[1,3*]

[1]Cardiovascular Research Institute, University of California, San Francisco, CA, USA

[2]Department of Pharmaceutical Chemistry, University of California, San Francisco, CA, USA

[3]Department of Physiology, University of California, San Francisco, CA, USA

*Correspondence: abigail.buchwalter@ucsf.edu

Abstract:

The inner nuclear membrane (INM), a subdomain of the endoplasmic reticulum (ER), sequesters hundreds of transmembrane proteins within the nucleus. We previously found that one INM protein, emerin, can evade the INM by secretory transport to the lysosome, where it is degraded. In this work, we used targeted mutagenesis to identify intrinsic sequences that promote or inhibit emerin's secretory trafficking. By manipulating these sequences across several tag and expression level combinations, we now find that emerin's localization is sensitive to C-terminal GFP tagging. While emerin's long, hydrophobic C-terminal transmembrane domain facilitates trafficking to the lysosome, extending its lumenal terminus with a GFP tag biases the protein toward this pathway. In contrast, we identify a conserved ER retention sequence that stabilizes N- and C-terminally tagged emerin by limiting its lysosomal flux. These findings underscore long-standing concerns about tagging artifacts and reveal novel determinants of tail-anchored INM protein targeting.

Introduction:

Tail-anchored proteins of the inner nuclear membrane (INM) are a unique class of transmembrane proteins with poorly understood biosynthesis, targeting, and degradation. The INM is a specialized extension of the endoplasmic reticulum (ER) membrane, the major site of membrane protein synthesis. Shortly after translation, tail-anchored proteins are embedded by their C-terminal transmembrane domains into the ER[1]. Unlike cytoplasmic tail-anchored proteins, which rapidly traffic out of the ER toward their target membranes, INM proteins must remain in the ER long enough to diffuse through the nuclear pore complex (NPC) and be retained by binding to nuclear structures[2,3]. This process repeats each time the nuclear envelope reforms at the end of mitosis[4]. INM proteins thus spend considerable time in the ER, but how they interact with the ER's secretory or proteostatic functions is unclear.

Our previous work identified emerin (EMD) as a short-lived INM protein in C2C12 mouse myoblasts[5]. While investigating how emerin is degraded, we found that C-terminally GFP-tagged emerin travels by vesicular transport to the plasma membrane (PM) and lysosome during ER stress. This unexpected secretory trafficking was prevented by the removal of EMD-GFP's N-terminal LEM domain, suggesting that this domain played a role in stress-induced lysosomal degradation. We hypothesized that the INM might dynamically respond to ER stress by shunting emerin through the secretory pathway to the lysosome. However, we now find that N-terminally GFP-tagged emerin traffics at a lower rate than C-terminally tagged emerin, and find no conclusive evidence that untagged emerin traffics to the lysosome. We also show that the secretory trafficking of tagged emerin depends on its unusually hydrophobic transmembrane domain (TMD). In isolation, the TMDs of both emerin and the related tail-anchored protein LAP2β readily traffic to the PM, but trafficking of the full-length tagged proteins is limited by a conserved RXR-type ER retention motif. Our experiments indicate that emerin's trafficking is artifactually expedited by C-terminal GFP tagging. However, these studies identify sequence elements that target emerin to the contiguous nuclear envelope/endoplasmic reticulum (NE/ER) network and highlight the interdependence between protein biogenesis, topology, and localization.

Results:

After our initial discovery, we aimed to understand the mechanism of emerin's secretory trafficking and its conservation across species, cell types, and expression levels. As our earlier experiments used C2C12 mouse myoblasts, we first tested whether EMD-GFP trafficking is conserved in human cells. We stably expressed tet-inducible mouse and human GFP fusions in human

osteosarcoma (U2OS) cells. When treated with the lysosome blocking agent bafilomycin A1 (BafA1), we found that U2OS cells, unlike C2C12 myoblasts[5], do not rely on ER stress to initiate secretory trafficking of EMD-GFP. Instead, BafA1 alone caused EMD-GFP to accumulate in lysosomal puncta. We used this high secretory flux to differentiate between emerin constructs that could and could not traffic (Figure 1A). Consistent with our C2C12 findings, we verified that WT EMD-GFP could traffic to the lysosome of U2OS cells, while a construct lacking the N-terminal LEM domain (ΔLEM, Figure 1B) could not. Our constructs were tagged with a C-terminal/lumenal GFP, which allowed us to quantify the proportion of EMD-GFP in the secretory pathway using cell surface antibody labeling and flow cytometry (Figure 1C,D). We calculated the trafficking level of each construct by dividing the surface anti-GFP antibody signal by the total EMD-GFP fluorescence. In line with our microscopy experiments, the anti-GFP antibody did not detect any ΔLEM construct at the PM of U2OS cells, while the WT EMD-GFP PM signal was always above background (Figure 1E).

Emerin's hydrophobic transmembrane domain is necessary and sufficient for trafficking of EMD-GFP

We further leveraged this U2OS system to examine how emerin's protein sequence facilitates trafficking. Emerin contains three major domains: an N-terminal LEM domain that interacts with the chromatin crosslinker BANF1/BAF, an intrinsically disordered region (IDR) that binds the nuclear lamina, and a C-terminal transmembrane domain (TMD)[6] (Figure 1B). We tested each domain's ability to traffic through the secretory pathway with a series of domain truncation experiments. Having established that removing the LEM domain abolished emerin's ability to traffic, we next deleted the disordered region between the LEM domain and the transmembrane domain (TMD). This construct (termed LEM-TMD) accumulated at the PM 10-fold more than the WT protein, indicating that the TMD, LEM domain, or both together are sufficient for trafficking (Figure 1F). To distinguish between these possibilities, we tested whether emerin's TMD alone can travel to the PM. We removed all but the TMD alpha helix and its surrounding 26 residues (mEMD 212-259), which we found to be required for membrane insertion of the truncated construct (not shown), and appended this TMD-only construct to either the C- or N-terminus of eGFP. Both TMD-GFP and GFP-TMD localized prominently to the ER and PM, and both were evident in the lysosome after BafA1 treatment (Figure 1F-G). These experiments reveal that emerin's TMD alone can traffic to the lysosome, regardless of GFP tag orientation.

We wondered what properties of emerin's TMD mediate its secretion. Tail-anchored proteins can sort via their TMDs along the secretory pathway[7–9]; long and hydrophobic sequences partition to the thicker, more hydrophobic membranes of the late secretory organelles[10] (Figure S2B-C), while tail-anchored proteins with shorter, less hydrophobic TMDs preferentially remain in the ER. We noticed that emerin's TMD is particularly hydrophobic among other NE/ER transmembrane domains (Figure S2A-B), which led us to predict that emerin's TMD is required for its exit from the ER. To test this, we replaced emerin's TMD with that of cytochrome B5, a model ER protein with a modestly hydrophobic TMD[11]. This substitution ablated trafficking through the secretory pathway (Figure 2A-B), indicating that emerin's TMD is indeed necessary for trafficking. We tested whether this depended on the hydrophobic content of the alpha helix by sequentially mutating its aromatic residues to alanine. We divided the TMD into N- and C-terminal halves, mutating three aromatic amino acids in each half (Figure 2C). The N-terminal TMD mutant was slightly less hydrophobic and had a greater effect on secretory trafficking than the C-terminal mutant (Figure 2D-E). Combining the N- and C-terminal mutations additively blocked trafficking, indicating that the number of aromatic residues in the TMD influences EMD-GFP's membrane partitioning.

Emerin contains a conserved ER retention signal

The autonomous trafficking of emerin's TMD challenged our initial hypothesis that emerin's localization relies on the LEM domain. Because EMD ΔLEM-GFP cannot traffic despite containing the TMD, we wondered whether a sequence within the ΔLEM construct inhibits trafficking. We noted that removing the LEM domain exposed a highly charged and conserved motif (QRRR) on the N-terminus of the construct (Figure S2D). Poly-arginine (RXR) motifs are known negative regulators of ER-to-Golgi transit[12]; we therefore tested whether this unprotected RXR could explain the ER-restricted localization of ΔLEM-GFP. Indeed, further truncating the ΔLEM construct by deleting the QRRR (ΔLEMΔQRRR) freed the protein from the ER (Figure 2F-H).

To test whether the RXR motif limits the trafficking of full length EMD-GFP, we mutated the QRRR to AAAA (designated RA) and detected more flux to the PM compared to WT EMD-GFP (Figure 2F-G). Both ΔLEMΔQRRR-GFP and EMD RA-GFP were less abundant at steady-state and were more rapidly degraded after removal of doxycycline from the medium (Figure 2I-J), suggesting increased flux to the lysosome. These data indicate that the RXR motif constitutes an ER retention sequence in EMD-GFP that is strengthened by the removal of the LEM domain. We infer that the presence of the LEM domain modulates the accessibility of the RRR motif; while the LEM domain

124 itself is in fact dispensable for trafficking, its removal constitutively exposes the RRR motif,
125 enhancing emerin's ER localization.
126
127 We next investigated the interplay between emerin's pro-trafficking TMD and its anti-trafficking
128 RXR motif by cloning the RA mutation into our TMD mutant constructs (see Figure 2C-E). The RA
129 mutation generally increased the surface expression of the TMD mutants except for the construct
130 with the lowest hydrophobicity score (TMD^m), which was not significantly altered by the RA
131 mutation (Figure 3A-B). We infer from this that the TMD acts upstream of the RXR motif in
132 emerin's secretory trafficking, fitting with the hypothesis that low TMD hydrophobicity suffices to
133 stably retain proteins in the ER[7].
134
135 Emerin is not the only tail-anchored INM protein with a particularly hydrophobic TMD. Another
136 such protein is LAP2β[13], which shares several sequence features with emerin[14] (Figure S2A, 3C).
137 We identified three RXR motifs within the LAP2β N-terminal domain, one of which (designated
138 RXR1) is just downstream of the LEM-like fold—a striking similarity to emerin's RXR motif (Figure
139 3C). To test whether the same localization mechanisms govern LAP2β, we tagged its C-terminus
140 with GFP and expressed it in U2OS cells. LAP2β-GFP was detected at the cell surface, albeit at
141 much lower levels than EMD-GFP (Figure 3D-E, S3A-B). Interestingly, replacing most of the
142 LAP2β N-terminal domain with the soybean ascorbate peroxidase (APEX2) enzyme caused a 20-
143 fold increase in PM expression (Figure 3D, S3B), suggesting that the LAP2β TMD has a similar
144 proclivity for secretory trafficking. Finally, mutating the LAP2β RXR1 to AAA led to a 70% increase
145 in PM accumulation (Figure 3D), mirroring the effect of the EMD RA mutation. Together, these
146 data indicate that the emerin and LAP2β TMDs are insufficient for NE/ER targeting and that both
147 proteins contain retention sequences which counteract TMD-dependent secretion.
148
149 RXR motifs are thought to bind COPI subunits to return escaped proteins to the ER[12,15], though
150 this mechanism is not understood. To test whether the increased trafficking of the RA mutant
151 results from reduced COPI interaction, we immunoprecipitated N-terminally FLAG-tagged mouse
152 emerin constructs from U2OS cells (Figure S3C). Mass spectrometry revealed a robust interaction
153 between emerin and the COPI coat, with several COPI subunits ranking among the top hits
154 (Figure 3F). Surprisingly however, this interaction was not weakened by the RXR mutation (Figure
155 3G). We noted that the mouse EMD bait also co-immunoprecipitated endogenous human EMD
156 (Figure 3G), opening the possibility that COPI might indirectly interact with both FLAG constructs

157 via endogenous emerin. Alternatively, the RXR motif's function could depend on protein topology.
158 Importantly, while we were able to detect FLAG-EMD in the lysosome by IF (Figure S3D), the
159 FLAG-RA construct was not poorly expressed relative to WT, in contrast with RA-GFP (Figures
160 S3C, 2I). We also noted that the lysosomal accumulation of N-terminally FLAG-tagged emerin
161 was more subtle than the C-terminally GFP-tagged version (Figures 1A, 2B), indicating that
162 epitope tagging and/or tag orientation influences the extent of emerin protein turnover.
163
164 **C-terminal tagging destabilizes emerin via secretory trafficking**
165 To determine whether tagging and/or overexpression increase the extent of emerin trafficking, we
166 needed a system to better control emerin expression. To this end, we generated a human iPSC
167 line with a dual integrase cassette exchange (DICE) landing pad[16] in the AAVS1 safe harbor locus
168 (Figure 4A), then knocked emerin out of these cells with CRISPR/Cas9 (Figure 4B). Integrating
169 GFP-tagged constructs into the parental and EMD KO DICE landing pads enabled us to measure
170 EMD-GFP trafficking in the presence or absence of the endogenous copy, respectively (Figure
171 4C). We included an mCherry-P2A upstream of the EMD-GFP to control for minor differences in
172 construct expression (Figure 4A). The GFP-tagged emerin constructs mirrored the trafficking
173 pattern we observed in U2OS cells; the EMD RA-GFP construct accumulated more at the PM,
174 while the TMD mutant did not traffic (Figure 4D-E). The steady state abundance reflected these
175 trafficking patterns. The GFP fluorescence of the TMD mutant accumulated to higher levels,
176 indicating that it was stabilized by its inability to traffic. In contrast, the RA mutant fluorescence
177 was slightly lower, indicating that it was modestly less stable than the WT protein, although this
178 difference is not statistically significant (Figure 4F-G). There was no difference in total or surface
179 expression between integrants in the EMD knockout and WT DICE backgrounds, suggesting that
180 the trafficking of EMD-GFP is comparable both when moderately overexpressed and when
181 expressed at endogenous levels (Figure 4D-E).
182
183 Tracking tail-anchored (i.e. untagged/N-terminally tagged) emerin through the secretory pathway
184 is challenging because it lacks a lumenal domain amenable to surface labeling. However, after
185 discovering ways to limit lysosomal flux (via the TMD) or accelerate it (via the RXR motif), we
186 reasoned that the trafficking patterns of tail-anchored mutants could be inferred from their steady
187 state abundance when expressed from the DICE landing pad. To test whether the GFP tag
188 orientation affects protein expression, we compared the steady state fluorescence of N- and C-
189 terminally tagged mutants. Surprisingly, the N-terminally tagged (tail-anchored) GFP fusions were
190 4-5 times more abundant than the C-terminally tagged (single pass) fusions (Figure 4F-G). C-

terminal fusions were also more completely relocalized to the lysosome after BafA1 than N-terminal fusions, where NE/ER EMD signal was still apparent (Figure S4A). Unlike the C-terminal fusions, the N-terminally tagged TMD mutant did not accumulate more than the N-terminally tagged WT protein, suggesting that N-terminally tagged emerin is not destabilized by trafficking. We interpret this finding with caution, as we observed a slight decrease in the level of the N-terminally tagged TMD mutant compared to WT (Figure 4G). Since the insertion of tail-anchored proteins relies on TMD hydrophobicity[1,17], improper targeting to the ER membrane due to TMD mutation would confound our conclusion that N-terminally tagged constructs undergo similarly low levels of trafficking. Interestingly, upon treatment with BafA1, the N-terminally tagged WT and RA constructs formed GFP+ lysosomal puncta, while the N-terminally tagged TMD mutant did not (Figure S4A). This suggests that N-terminally tagged emerin does undergo some level of TMD-dependent trafficking. Further, the N-terminal RA fusion was slightly less fluorescent at steady state than WT (Figure 4G), indicating that the RXR motif also stabilizes tail-anchored GFP-EMD. Collectively, these data indicate that N- and C-terminally tagged emerin constructs travel to the lysosome via their hydrophobic TMDs, although C-terminal tags accelerate this trafficking.

Finally, we integrated untagged WT, RA, and TMD mutant constructs into EMD KO landing pad cells, then fixed and stained cells for confocal microscopy and flow cytometry. We saw no apparent differences in the localization or intensity of any of the emerin mutants, though the data were considerably noisier than the steady state GFP measurements (Figure 4H). We were also unable to detect untagged emerin in the lysosome after BafA1 treatment (Figure S4B), suggesting it does not traffic through the secretory pathway. However, the sensitivity of these assays may be limited by fixation, permeabilization, and antibody staining; therefore, we cannot rule out the possibility that small differences do exist between untagged emerin variants.

Discussion

In this work, we dissected how exogenous epitope tags and intrinsic sequence elements influence the secretory trafficking of the INM resident protein emerin. We discovered that the aromatic amino acids in emerin's 23-residue TMD facilitate its travel to the lysosome. In the absence of other signals, TMD length and hydrophobicity are sufficient to partition tail-anchored proteins along the secretory pathway[7,8]. The biophysical properties of the emerin and LAP2β TMDs resemble PM, rather than ER, resident TMDs (Figure S2, ref.[10]). However, this notable hydrophobicity is likely important for the proteins' biogenesis. Tail-anchored proteins with very hydrophobic transmembrane domains are post-translationally targeted by the TRC40/GET

complex, which captures C-terminal alpha helices after they emerge from the ribosome and delivers them to the ER membrane[1]. Emerin and Lap2β are established TRC40 client proteins[18,19], so their hydrophobic TMDs are likely required for TRC40 recognition. However, adding a C-terminal GFP converts a tail-anchored protein to a single-pass transmembrane protein, which are instead co-translationally targeted to the ER by the SRP pathway[17,20]. Our results indicate that this change in topology displaces emerin, making C-terminally tagged emerin less stable and more prone to lysosomal trafficking than its N-terminally tagged counterpart (Figure 4F-G, S4A). This suggests that hydrophobic TMDs are less energetically favored within the ER membrane when attached to a lumenal domain, or that different biogenesis pathways bias cargoes toward ER exit.

We hypothesize that active ER retention plays a role in INM protein targeting. In interphase, emerin is not entirely sequestered at the INM by the nuclear lamina; a pool of emerin protein remains in the peripheral ER[21,22]. The intrinsic ability of emerin's TMD to traffic from the ER implies that a limiting mechanism must exist to bias the protein toward diffusion to the INM. Emerin could stably reside in the ER in part by binding to other ER-resident proteins. Interestingly, emerin was reported to interact with the ER tethering protein MOSPD3 via its YEESY (95-99) motif[23], which we previously found to limit trafficking[5]. While both TMDs traffic to the plasma membrane, full-length LAP2β-GFP is more retained in the NE/ER than EMD-GFP (Figure 3D, S3A-B), indicating that the N-terminal domains limit trafficking to different extents.

We identified the RXR motif as a shared negative regulator of TMD-dependent trafficking, prompting us to revise our original model: the exposure of this motif, not the absence of the LEM domain, prevents ER exit of EMD-GFP (Figure 2F-G). This suggests that the sequences around the RXR motif influence its activity by steric occlusion or other mechanisms. RXR motifs prevent the ER exit of some PM-resident proteins until they are masked by oligomerization, thus coupling ER exit to folding and/or assembly[12]. Like the canonical ER retrieval motif KKXX, RXR motifs are thought to engage COPI subunits to return escaped ER membrane proteins from the early Golgi[12,24]. Yeast-2-hybrid experiments predicted RXR signals to interact with the beta and delta subunits of the COPI coat[15], though the molecular details are still unclear. Contrary to KKXX motifs, found only on C-termini, RXR motifs may be on N-termini or within a poly-peptide chain[12]. Truncated, lumenally tagged variants of Sun2, another tail-anchored INM protein, require a poly-arginine motif to prevent mislocalization to the Golgi[25]. Turgay et al[25]. observed purified Sun2 RXR mutants losing interaction with COPI subunits in GST pull-down assays. In contrast, we did not

observe loss of COPI binding in our RXR mutant immunoprecipitations. This discrepancy may be explained by differences in methods (purified recombinant protein binding assays vs. native IP), or by oligomerization of tagged emerin with endogenous emerin to indirectly bind COPI in lysate[26]. Emerin's interaction with the COPI coat was recently detected by proximity biotinylation in mouse P19 cells[27]. Interestingly, emerin was the only non-Golgi resident protein identified in the gamma-COP subunit interactome, indicating that endogenous emerin might be a COPI cargo. While we predict this interaction occurs via emerin's RXR motif, we cannot exclude the possibility of other COPI-interacting mechanisms.

Our previous work identified EMD as an unstable protein subject to significant lysosomal flux[5]. However, we have now discovered that emerin's trafficking is markedly promoted by C-terminal GFP tagging, likely influencing many of our initial observations. While we used C-terminal tags to avoid disrupting emerin's N-terminal interactions with chromatin and lamins, this approach inadvertently altered its localization. We did detect trafficking of N-terminally tagged emerin, but found that it occurs at a much lower rate. We conclude that hydrophobic tail-anchored transmembrane domains are readily dislocated by C-terminal tags, and echo the warnings raised by generations of cell biologists regarding tag-induced localization artifacts[28–31]. We did not detect trafficking of the untagged emerin constructs. Nonetheless, because trafficking is detectable at or below endogenous levels with different tags and orientations, we cannot rule out the possibility that emerin traffics under specific conditions. We note poor correlation of emerin transcript and protein across tissues[32] (Figure S4C), which suggests protein-level regulation that may dynamically regulate emerin levels. While we still do not know whether emerin's ability to travel beyond the NE/ER influences its function, our experiments reveal an unanticipated connection between the topology and localization of INM proteins and raise new questions about the balance between secretion and retention of INM-destined proteins.

Methods:

Cell culture and cell line generation:

U2OS cells were obtained from the UCSF Cell and Genome Engineering Core and were cultured in McCoy's 5A medium supplemented with 10% FBS and penicillin/streptomycin. To generate EMD-GFP cell lines, U2OS were seeded into 6-well plates at a density of 300,000 cells per well. The next day, a transfection mix of 0.5 ug EMD-GFP donor plasmid, 0.25 ug PB200A-1 PiggyBac Transposase plasmid, 3.5 uL Lipofectamine 2000, and 300 uL Optimem was added to each well. After 24 hours, cells were split 1:2 and selected in 5 ug/mL blasticidin for 1 week, then maintained

293 in 5 ug/mL blasticidin thereafter. Prior to an experiment, cells were split into media without
294 blasticidin and induced with 1 ug/mL doxycycline for 24-48 hours. To generate FLAG-EMD cell
295 lines, 2 ug CMV-FLAG-EMD plasmid was transfected without PiggyBac Transposase. Cells were
296 selected with 400 ug/mL G418 for one week, then maintained in 200 ug/mL G418.
297
298 WTC-11 hiPSCs were obtained from the Berkeley Stem Cell Center. Cells were maintained on
299 Matrigel-coated vessels in mTeSR+ without penicillin/streptomycin. Cells were passaged as
300 clumps (using ReLeSR) for routine culture and as single cells (using Accutase) for counting and
301 electroporating. Cells were plated in ROCK inhibitor Y-27632, then changed to fresh mTeSR+
302 after 24 hours. CRISPR editing was performed by electroporating 12.5 pmol pure Cas9-NLS and
303 12.5 pmol sgRNA into 1 million cells using a 100 uL Neon electroporator set to 1300 V, 30 ms,
304 and 1 pulse. For DICE landing pad installation, we included 2 ug cassette-containing HDR
305 template plasmid in the transfection mix. Landing pad cells were selected in 0.25 ug/mL
306 puromycin for 3 days. Single clones were isolated by limiting dilution in 96 well plates, then
307 expanded and genotyped for heterozygous insertion using primers spanning the AAVS1
308 homology arms. Emerin knockouts were generated from one landing pad clone using two sgRNAs
309 targeting the start and end of the coding sequence. Clones were genotyped by PCR to verify the
310 entire region was deleted, then by Western blot to confirm the loss of protein. To integrate emerin
311 constructs into the DICE landing pad, we electroporated 1 million cells with 2 ug attB-containing
312 donor plasmid and 500 ng BxbI-P2A-PhiC31 integrase plasmid. After letting cells recover, we
313 isolated landing pad BFP–/donor+ cells using a SONY SH800 cell sorter. Cells were checked for
314 mycoplasma every 3-4 months and were found to be negative.
315
316 **Plasmid cloning:**
317 All U2OS constructs except FLAG-EMD were expressed in the XLone all-in-one Tet-ON Piggybac
318 plasmid[33]. Mouse emerin sequences were cloned into XLone from plasmids used in our previous
319 study. Human emerin and LAP2β were amplified from Hek293T and WTC-11 cDNA using primers
320 with overhangs to XLone. Mouse cytochrome B5 was amplified from E14 mESC cDNA. cDNA
321 was synthesized using NEB MMLV reverse transcriptase. FLAG-EMD constructs were expressed
322 from the CMV promoter in a Neo/Kan resistant vector.
323

324 **Emerin constructs:**

Designation	Gene	Species	Uniprot ID	Mutation
LAP2β RXR1	LAP2β	Human	P42167	48-50 -> AAA
LAP2β APEX2-TMD	LAP2β	Human	P42167	1-280 -> APEX2
hEMD RA	EMD	Human	P50402	44-47 -> AAAA
hEMD ΔLEM		Human Mouse	P50402 O08579	D1-43
hEMD ΔLEM ΔQRRR	EMD	Human Mouse	P50402 O08579	D1-47
hEMD Cyb5 TM	EMD	Human	P50402 (EMD) P56395 (Cyb5)	EMD 1-224 + mouse cyb5a 95-134
mEMD Cyb5 TM	EMD	Mouse	O08579 (EMD) P56395 (Cyb5)	EMD 1-225 + mouse Cyb5a 95-134
TMD-GFP	EMD	Mouse	O08579	212-259
N-TMDm	EMD	Human	P50402	W226A ,F232A, F235A
C-TMDm	EMD	Human	P50402	F240A, F241A, Y243A
Full TMDmut	EMD	Human	P50402	W226A ,F232A, F235A, F240A, F241A, Y243A

325

326 Small emerin mutations were generated using the NEB site-directed mutagenesis kit, while larger
327 fusions were assembled using the NEB HiFi Assembly kit.
328 The DICE landing pad cassette contained a PGK promoter driving HSV thymidine kinase-P2A-
329 TagBFP, all flanked by BxbI and PhiC31 attP sites. This cassette was built into an AAVS1 targeting
330 vector (a generous gift from Dr. Tom Nowakowski) containing a splice acceptor-P2A-puro. DICE
331 donor constructs contained Bxb1 and PhiC31 attB sites flanking the CAGGS promoter and an
332 mCherry-P2A-EMD.
333 Plasmids were prepped using the ZymoPURE II midiprep kit. All plasmids were verified by Sanger
334 or whole plasmid nanopore sequencing before transfection.
335

336 **Transmembrane domain hydrophobicity calculations:**
337 Transmembrane segments were obtained for EMD, LAP2β, STX3, and CYB5 from Uniprot
338 annotations. DG-ins was calculated using the DGprediction algorithm[34]. Median DG-transfer and

339 TM length values for secretory membranes were obtained from the human Membranome
340 database[13,35]. Data obtained from the Membranome database were plotted in GraphPad Prism.
341
342 **Surface labeling and flow cytometry:**
343 The surface staining assay was adapted from Welch et al[36]. Briefly, cells were washed with PBS,
344 lifted for 3-5 minutes with accutase, then quenched with cold complete media. Cells were
345 transferred to microfuge tubes and placed on ice for the duration of staining and washing. Cells
346 were pelleted 800g for 3 minutes at 4C, then washed once in 2% FBS/PBS. Cells were stained
347 in 80 uL anti-GFP 647 (1:20 in 2% FBS/PBS) or anti-rabbit IgG Alexa Fluor 647 secondary
348 antibody (1:200 in 2% FBS/PBS) as a negative control. The cells used for the anti-IgG controls
349 were WT EMD-GFP (for all EMD comparisons) or WT LAP2β-GFP (for LAP2β comparisons). After
350 staining for 30 minutes, cells were diluted with 200 uL 2% FBS/PBS, pelleted and washed twice
351 with 400 uL 2% FBS/PBS, and then optionally fixed in 4% PFA/PBS for 10 minutes at room
352 temperature. Fixed cells were washed twice and then stored at 4C until being resuspended in
353 PBS and strained into round bottom FACS tubes before analysis.
354
355 For flow analysis of antibody-stained proteins, cells were lifted with accutase, washed with PBS,
356 and fixed by rotating in 4% PFA/PBS for 10 minutes. After washing twice in PBS, cells were
357 permeabilized in IF buffer (0.1% Tx100, 0.02% SDS, 10 mg/ml BSA in PBS) for 30 minutes before
358 incubating in primary antibody solution for 1-2 hours at room temperature. Cells were washed
359 three times in IF buffer, incubated with fluorescent secondary antibodies for 1 hour, and then
360 washed three more times before being strained into FACS tubes.
361
362 Cells were analyzed on a BD FACSVerse or a ThermoFisher Attune NxT. At least 50,000 cells
363 were analyzed per sample. Flow cytometry data were analyzed in FlowJo. Surface antibody:GFP
364 ratio was obtained using the “derive parameters” function and applied to the GFP+ populations.
365 Histograms are normalized to the mode of each sample for visualization.
366
367 **Immunofluorescence microscopy:**
368 Cells were seeded in Ibidi culture chambers (Matrigel-coated for hiPSCs) prior to an IF
369 experiment. For lysosome colocalization analysis, cells were treated with 100 nM bafilomycin A1
370 for 16-18 hours. Cells were washed in PBS, then fixed in 4% paraformaldehyde in PBS for 5
371 minutes at room temperature. For LAMP1 staining, cells were permeabilized in 0.1%
372 digitonin/PBS at 4 C for 10 minutes, then blocked in 2% FBS/PBS. LAMP1 antibody was diluted

373 1:200 in 2% FBS/PBS. For emerin and FLAG immunostaining, fixed cells were permeabilized in
374 IF buffer for 30 minutes, then incubated in primary antibodies (diluted 1:250 and 1:1000 in IF
375 buffer, respectively) for 1 hour at room temperature. After washing, cells were incubated with
376 Alexa-Fluor-conjugated secondary antibodies and Hoechst 33342 (both 1:1000) for 30 minutes
377 at room temperature. Emerin/FLAG staining is incompatible with LAMP1 staining because of
378 differential permeabilization requirements. In these cases, we had to rely on the formation of
379 EMD+ puncta after bafilomycin treatment to infer lysosome localization.

380 Images were acquired using a Nikon CSU-X1 spinning disk confocal microscope with 40x/1.3
381 NA or 60x/1.4 NA oil objectives. 20-30 Z-slices were imaged per cell with a step size of 0.3
382 microns. 16-bit images were saved as ND2 files using the Nikon Elements 5.02 build 1266
383 software. Representative slices were selected and cropped in FIJI.

384

385 **Protein stability measurement and Western blotting:**

386 For doxycycline washout experiments, 300,000 U2OS cells were seeded in 12 well plates with 2
387 ug/mL doxycycline. After 48 hours, half the wells were washed twice with PBS and incubated in
388 fresh medium without doxycycline for 18 hours. Cells were washed twice with PBS and lysed in
389 the wells by scraping in 80 uL RIPA buffer (50mM Tris, 150mM NaCl, 1% TritonX-100, 0.5%
390 deoxycholate, 0.1% SDS) plus protease inhibitors and benzonase. Lysates were spun 17,000g
391 at 4C for 10 minutes, then supernatants were mixed with sample buffer and boiled for 10
392 minutes. 12 uL of each sample was loaded onto homemade 10% SDS-PAGE gels, then
393 transferred onto nitrocellulose membranes. Blots were incubated at 4C overnight in primary
394 antibody diluted with 5% milk/TBST, then washed and incubated in HRP-conjugated secondary
395 antibodies for 1 hour at room temperature. Blots were developed using Pierce ECL Western
396 blotting substrate and imaged using the GelDoc imaging system. Band intensity was quantified
397 in Fiji.

398

399 **FLAG-EMD immunoprecipitation and mass spectrometry**

400 FLAG-EMD, FLAG-RA, and parental U2OS (non-expressing negative control) cells were grown
401 to confluence in 3 10cm plates per cell line, then harvested by scraping and transferring to a
402 microfuge tube. Cells were pelleted and lysed in 1 mL lysis buffer (50 mM Tris-HCl pH 7.4, 150
403 mM NaCl, 0.3% TritonX-100, 1 mM DTT, 2 mM EDTA, 5 mM MgCl2, 1x protease inhibitor cocktail,
404 1x PhosSTOP, benzonase), then incubated for 30 minutes end over end at 4C. Lysates were
405 probe sonicated in 6 rounds of 10 second pulses at 20% power, then spun 17,000g at 4C for 25

minutes. The supernatant was added to 40 uL FLAG M2 magnetic beads which had been calibrated in 500 uL lysis buffer and separated on a magnetic stand. Samples were incubated end over end at room temperature for 1 hour, then magnetically separated and washed 3 times with 1 mL wash buffer (100 mM HEPES-KOH pH 7.5, 100 mM KCl, 5% glycerol, 0.1% NP-40, protease inhibitors). After the final wash, the supernatant was discarded and the beads were resuspended in 200 uL elution buffer (100 ug/mL 3x FLAG peptide in wash buffer) and eluted for 1 hour at room temperature. Eluates were precipitated with 4 volumes ice cold acetone overnight at -20C, spun at max speed for 5 minutes, then air dried. Pellets were processed for mass spectrometry using a PreOmics iST kit according to manufacturer's instructions.

Mass spectrometry and analysis

A nanoElute was attached in line to a timsTOF Pro equipped with a CaptiveSpray Source (Bruker, Hamburg, Germany). Chromatography was conducted at 40°C through a 25 cm reversed-phase C18 column (PepSep) at a constant flowrate of 0.5 µL min^{-1}. Mobile phase A was 98/2/0.1% water/MeCN/formic acid (v/v/v) and phase B was MeCN with 0.1% formic acid (v/v). During a 108 min method, peptides were separated by a 3-step linear gradient (5% to 30% B over 90 min, 30% to 35% B over 10 min, 35% to 95% B over 4 min) followed by a 4 min isocratic flush at 95% for 4 min before washing and a return to low organic conditions. Experiments were run as data-dependent acquisitions with ion mobility activated in PASEF mode. MS and MS/MS spectra were collected with *m*/*z* 100 to 1700 and ions with $z = +1$ were excluded. Raw data files are available on the Mass Spectrometry Interactive Virtual Environment (MassIVE), a full member of the Proteome Xchange consortium under the identifier: MSV000096858.

Raw data files were searched using PEAKS Online Xpro 1.6 (Bioinformatics Solutions Inc., Waterloo, Ontario, Canada). The precursor mass error tolerance and fragment mass error tolerance were set to 20 ppm and 0.03 respectively. The trypsin digest mode was set to semi-specific and missed cleavages was set to 2. The human Swiss-Prot reviewed (canonical) database (downloaded from UniProt) totaling 20,385 entries or a custom database using human and mouse emerin (downloaded from uniprot, EMD_human P50402, EMD_mouse O08579) was used. Carbamidomethylation (C) was selected as a fixed modification. Oxidation (M) was selected as a variable modification.

Resulting datasets were subjected to the following filtration criteria: (1) Database search ($-10 \log(p\text{-value}) \geq 20$, 1% peptide and protein FDR). (2) Identified proteins with less than 3%

coverage, 3 unique peptides, or spectral areas less than 5000 were discarded. (4) Spectral counts for each protein were normalized to corresponding counts from the negative control IP, and then to the protein length. (5) The ratio of normalized counts to the mouse emerin bait was plotted to obtain relative co-immunoprecipitation efficiency.

Acknowledgements

We are grateful to UCSF core facility staff for training and technical support. The Gladstone Institutes Stem Cell Core provided hiPSC culture training and equipment. Images were acquired at the Center for Advanced Light Microscopy- CVRI Microscopy core on microscopes purchased though the UCSF Research Evaluation and Allocation Committee, the Gross Fund, and the Heart Anonymous Fund. Flow cytometers and cell sorters were purchased and supported by the UCSF Center for Live Cell Analysis core.

We also thank Elphege Nora for guidance with integrase cassette exchange, Emmy Delaney for experimental assistance, and Tracy Knight for experimental assistance and feedback on this manuscript. Adam Frost, Shaeri Mukherjee, Peter Walter, Martin Kampmann, Willow Coyote-Maestas, and members of the Buchwalter lab provided valuable perspective and discussion throughout this work.

A.B. was supported by the Chan Zuckerberg Biohub, and J.M. was supported by the National Heart, Lung, and Blood Institute (F31HL170757).

References

1. Rapaport, D. & Herrmann, J. M. Chasing the right tail: How the ER membrane complex recognizes its substrates. *Journal of Cell Biology* **222**, e202306035 (2023).
2. Boni, A. *et al.* Live imaging and modeling of inner nuclear membrane targeting reveals its molecular requirements in mammalian cells. *Journal of Cell Biology* **209**, 705–720 (2015).
3. Ungricht, R., Klann, M., Horvath, P. & Kutay, U. Diffusion and retention are major determinants of protein targeting to the inner nuclear membrane. *J Cell Biol* **209**, 687–704 (2015).
4. Ellenberg, J. *et al.* Nuclear Membrane Dynamics and Reassembly in Living Cells: Targeting of an Inner Nuclear Membrane Protein in Interphase and Mitosis. *J Cell Biol* **138**, 1193–1206 (1997).
5. Buchwalter, A., Schulte, R., Tsai, H., Capitanio, J. & Hetzer, M. Selective clearance of the inner nuclear membrane protein emerin by vesicular transport during ER stress. *eLife* **8**, e49796 (2019).
6. Lee, K. K. *et al.* Distinct functional domains in emerin bind lamin A and DNA-bridging protein BAF. *Journal of Cell Science* **114**, 4567–4573 (2001).
7. Ronchi, P., Colombo, S., Francolini, M. & Borgese, N. Transmembrane domain–dependent partitioning of membrane proteins within the endoplasmic reticulum. *J Cell Biol* **181**, 105–118 (2008).
8. Borgese, N. Getting membrane proteins on and off the shuttle bus between the endoplasmic reticulum and the Golgi complex. *Journal of Cell Science* **129**, 1537–1545 (2016).
9. Bulbarelli, A., Sprocati, T., Barberi, M., Pedrazzini, E. & Borgese, N. Trafficking of tail-anchored proteins: transport from the endoplasmic reticulum to the plasma membrane and sorting between surface domains in polarised epithelial cells. *Journal of Cell Science* **115**, 1689–1702 (2002).

482 10. Sharpe, H. J., Stevens, T. J. & Munro, S. A Comprehensive Comparison of
483 Transmembrane Domains Reveals Organelle-Specific Properties. *Cell* **142**, 158–169 (2010).
484 11. E, P., A, V., R, L., A, B. & N, B. Mechanism of residence of cytochrome b(5), a tail-
485 anchored protein, in the endoplasmic reticulum. *J Cell Biol* **148**, 899–914 (2000).
486 12. Michelsen, K., Yuan, H. & Schwappach, B. Hide and run. *EMBO Rep* **6**, 717–722 (2005).
487 13. Lomize, A. L., Lomize, M. A., Krolicki, S. R. & Pogozheva, I. D. Membranome: a
488 database for proteome-wide analysis of single-pass membrane proteins. *Nucleic Acids Res*
489 **45**, D250–D255 (2017).
490 14. Berk, J. M., Tifft, K. E. & Wilson, K. L. The nuclear envelope LEM-domain protein emerin.
491 *Nucleus* **4**, 298–314 (2013).
492 15. Michelsen, K. *et al.* Novel cargo-binding site in the β and δ subunits of coatomer. *Journal*
493 *of Cell Biology* **179**, 209–217 (2007).
494 16. Zhu, F. *et al.* DICE, an efficient system for iterative genomic editing in human pluripotent
495 stem cells. *Nucleic Acids Research* **42**, e34 (2014).
496 17. Shao, S. & Hegde, R. S. Membrane Protein Insertion at the Endoplasmic Reticulum.
497 *Annu Rev Cell Dev Biol* **27**, 25–56 (2011).
498 18. Coy-Vergara, J., Rivera-Monroy, J., Urlaub, H., Lenz, C. & Schwappach, B. A trap
499 mutant reveals the physiological client spectrum of TRC40. *J Cell Sci* **132**, jcs230094 (2019).
500 19. Pfaff, J. *et al.* Emery–Dreifuss muscular dystrophy mutations impair TRC40-mediated
501 targeting of emerin to the inner nuclear membrane. *J Cell Sci* **129**, 502–516 (2016).
502 20. Translocation of proteins across the endoplasmic reticulum. I. Signal recognition protein
503 (SRP) binds to in-vitro-assembled polysomes synthesizing secretory protein. *J Cell Biol* **91**,
504 545–550 (1981).
505 21. Nastały, P. *et al.* Role of the nuclear membrane protein Emerin in front-rear polarity of
506 the nucleus. *Nature Communications* **11**, 2122 (2020).

22. Salpingidou, G., Smertenko, A., Hausmanowa-Petrucewicz, I., Hussey, P. J. & Hutchison, C. J. A novel role for the nuclear membrane protein emerin in association of the centrosome to the outer nuclear membrane. *J Cell Biol* **178**, 897–904 (2007).

23. Cabukusta, B. *et al.* Human VAPome Analysis Reveals MOSPD1 and MOSPD3 as Membrane Contact Site Proteins Interacting with FFAT-Related FFNT Motifs. *Cell Reports* **33**, 108475 (2020).

24. Marcello, E., Gardoni, F., Luca, M. D. & Pérez-Otaño, I. An Arginine Stretch Limits ADAM10 Exit from the Endoplasmic Reticulum *. *Journal of Biological Chemistry* **285**, 10376–10384 (2010).

25. Turgay, Y. *et al.* A classical NLS and the SUN domain contribute to the targeting of SUN2 to the inner nuclear membrane. *The EMBO Journal* **29**, 2262–2275 (2010).

26. Fernandez, A., Bautista, M. & Pinaud, F. Emerin oligomerization and nucleoskeletal coupling at the nuclear envelope regulate nuclear mechanics against stress. *bioRxiv* 2021.02.12.429834 (2021) doi:10.1101/2021.02.12.429834.

27. Zhao, X. *et al.* ultraID: a compact and efficient enzyme for proximity-dependent biotinylation in living cells. 2021.06.16.448656 Preprint at https://doi.org/10.1101/2021.06.16.448656 (2021).

28. Stadler, C. *et al.* Immunofluorescence and fluorescent-protein tagging show high correlation for protein localization in mammalian cells. *Nat Methods* **10**, 315–323 (2013).

29. Montecinos-Franjola, F., Bauer, B. L., Mears, J. A. & Ramachandran, R. GFP fluorescence tagging alters dynamin-related protein 1 oligomerization dynamics and creates disassembly-refractory puncta to mediate mitochondrial fission. *Sci Rep* **10**, 14777 (2020).

30. Margolin, W. The Price of Tags in Protein Localization Studies. *J Bacteriol* **194**, 6369–6371 (2012).

531 31. Meyer, T., Begitt, A. & Vinkemeier, U. Green fluorescent protein-tagging reduces the
532 nucleocytoplasmic shuttling specifically of unphosphorylated STAT1. *The FEBS Journal* **274**,
533 815–826 (2007).
534 32. Wang, D. *et al.* A deep proteome and transcriptome abundance atlas of 29 healthy
535 human tissues. *Mol Syst Biol* **15**, e8503 (2019).
536 33. Randolph, L. N., Bao, X., Zhou, C. & Lian, X. An all-in-one, Tet-On 3G inducible
537 PiggyBac system for human pluripotent stem cells and derivatives. *Sci Rep* **7**, 1549 (2017).
538 34. Hessa, T. *et al.* Molecular code for transmembrane-helix recognition by the Sec61
539 translocon. *Nature* **450**, 1026–1030 (2007).
540 35. Lomize, A. L., Hage, J. M. & Pogozheva, I. D. Membranome 2.0: database for proteome-
541 wide profiling of bitopic proteins and their dimers. *Bioinformatics* **34**, 1061–1062 (2018).
542 36. Welch, L. G., Peak-Chew, S.-Y., Begum, F., Stevens, T. J. & Munro, S. GOLPH3 and
543 GOLPH3L are broad-spectrum COPI adaptors for sorting into intra-Golgi transport vesicles.
544 *Journal of Cell Biology* **220**, (2021).
545

Figure 1

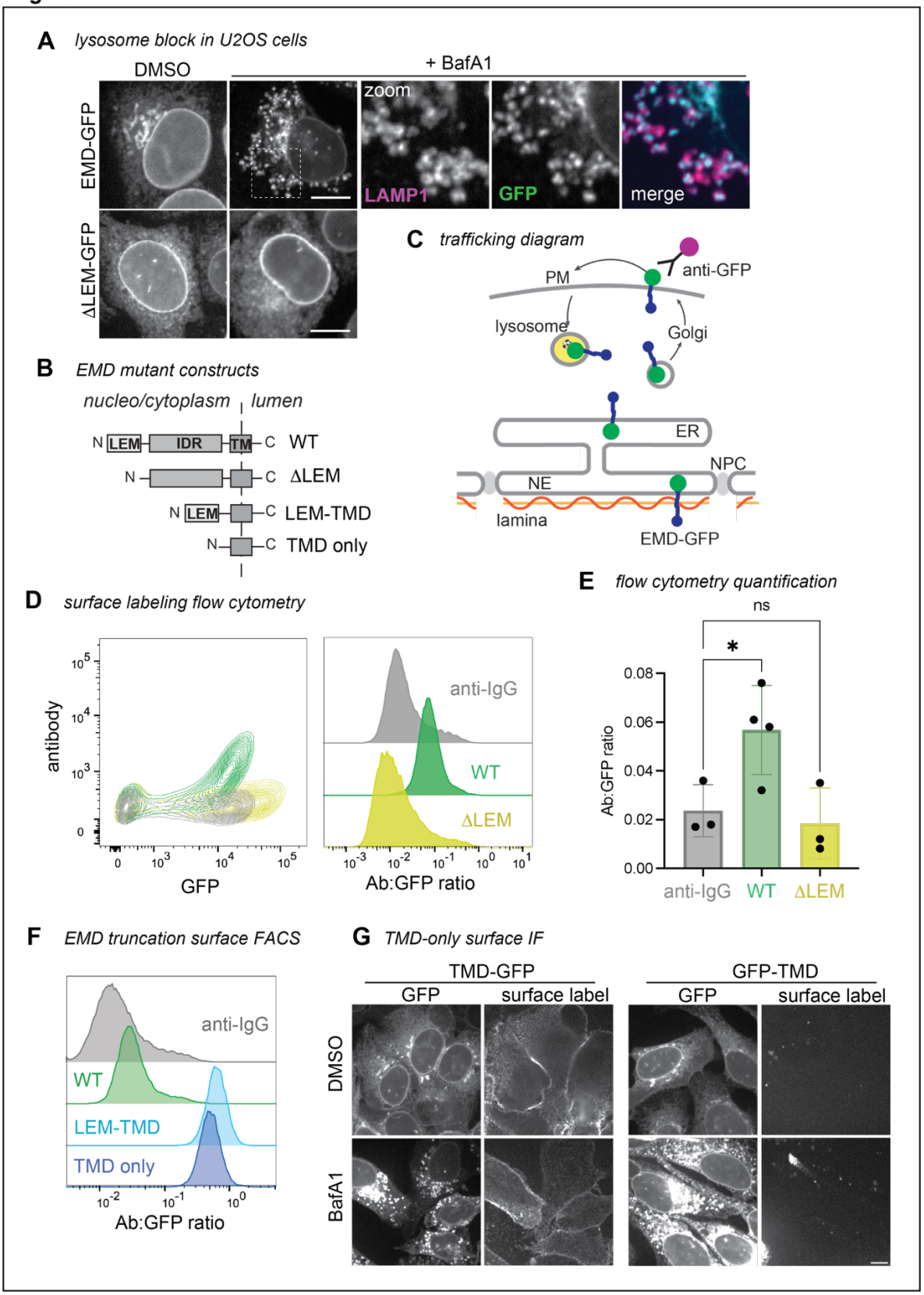
A lysosome block in U2OS cells
DMSO
+ BafA1
EMD-GFP
ΔLEM-GFP
zoom
LAMP1
GFP
merge
B EMD mutant constructs
nucleo/cytoplasm
lumen
N LEM IDR TM C WT
N C ΔLEM
N LEM C LEM-TMD
N C TMD only
C trafficking diagram
PM
anti-GFP
lysosome
Golgi
ER
NPC
NE
lamina
EMD-GFP
D surface labeling flow cytometry
antibody
GFP
anti-IgG
WT
ΔLEM
Ab:GFP ratio
E flow cytometry quantification
ns
*
Ab:GFP ratio
anti-IgG
WT
ΔLEM
F EMD truncation surface FACS
anti-IgG
WT
LEM-TMD
TMD only
Ab:GFP ratio
G TMD-only surface IF
TMD-GFP
GFP-TMD
GFP
surface label
DMSO
BafA1

Figure 1. EMD ΔLEM does not traffic in U2OS cells, while the TMD alone does.

A) U2OS cells expressing mouse EMD-GFP and ΔLEM-GFP were induced with 1 ug/mL doxycycline for 24 hours, treated with 100nM lysosome blocking agent Bafilomycin A1 (BafA1) overnight, and fixed and stained for lysosome marker Lamp1. Scale bar, 10 um.

B) Summary of EMD domains and truncation mutants.

C) EMD enriches at the INM by binding to the nuclear lamina, or exits the ER into the secretory pathway. Before reaching the lysosome, EMD transiently accesses the cell surface where lumenal GFP is exposed to anti-GFP antibody.

D) Example FACS plot of mouse WT vs ΔLEM surface labeling; fluorescent anti-IgG secondary antibody included as background control. Antibody signal is divided by total GFP+ signal to yield histograms on the right.

E) Quantification of the antibody:GFP ratio from 4 independent experiments, with error bars representing SD. * indicates adjusted P-value = 0.0451 by one-way ANOVA with Šídák's multiple comparisons test.

F) U2OS cells expressing mouse TMD-GFP (lumenal tag) or GFP-TMD (cytosolic tag) were treated overnight with BafA1, then fixed and stained with an anti-GFP antibody.

G) Example surface labeling FACS histogram of U2OS cells expressing WT, LEM-TMD-GFP, or TMD-GFP.

Figure 2

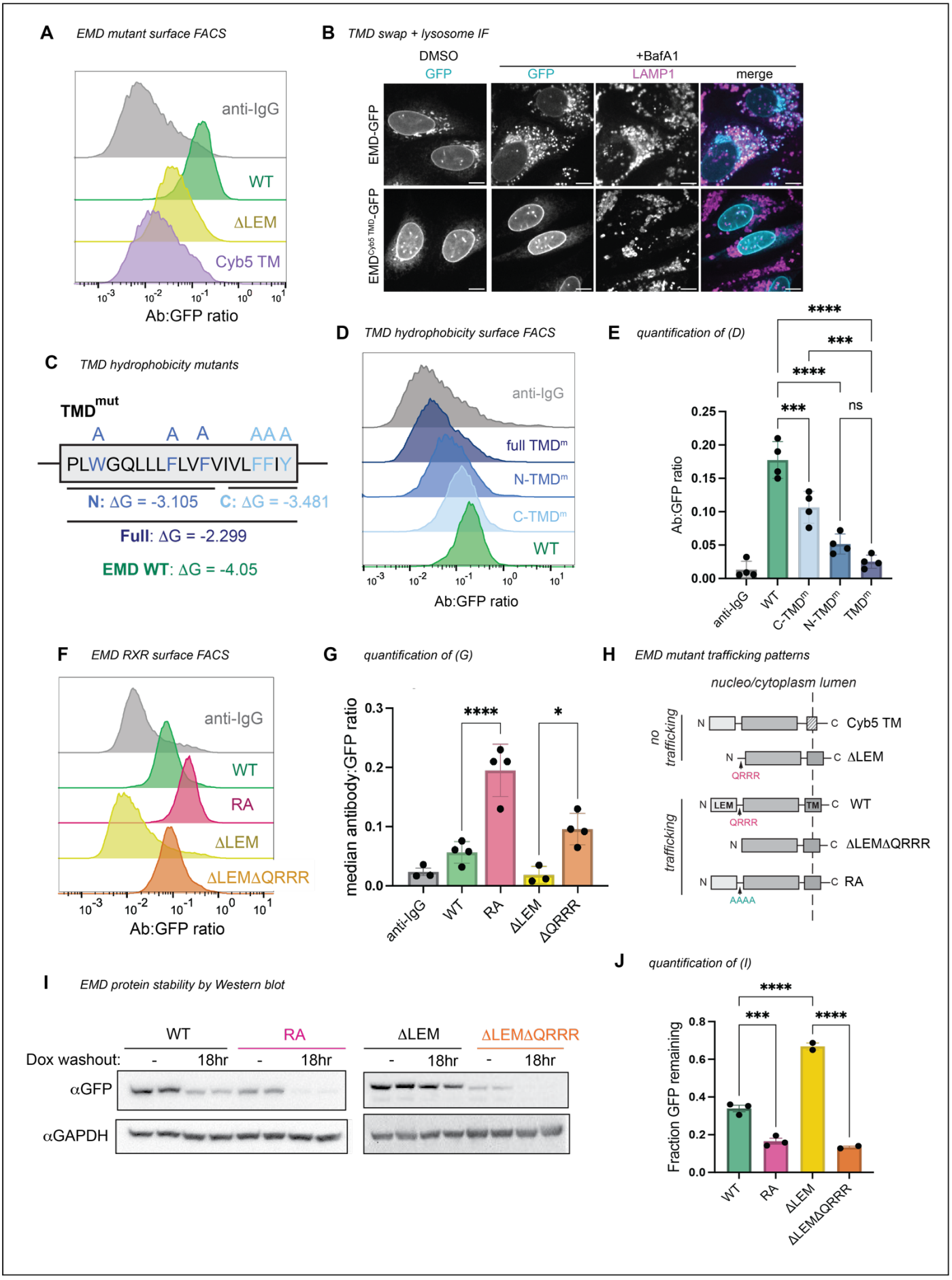
A
EMD mutant surface FACS
anti-IgG
WT
ΔLEM
Cyb5 TM
Ab:GFP ratio
B
TMD swap + lysosome IF
DMSO
+BafA1
GFP
GFP
LAMP1
merge
EMD-GFP
EMDCyb5 TMD-GFP
C
TMD hydrophobicity mutants
TMDmut
A A A AAA
PLWGQLLLFLVFVIVLFFIY
N: ΔG = -3.105
C: ΔG = -3.481
Full: ΔG = -2.299
EMD WT: ΔG = -4.05
D
TMD hydrophobicity surface FACS
anti-IgG
full TMDm
N-TMDm
C-TMDm
WT
Ab:GFP ratio
E
quantification of (D)
Ab:GFP ratio
anti-IgG
WT
C-TMDm
N-TMDm
TMDm
ns
F
EMD RXR surface FACS
anti-IgG
WT
RA
ΔLEM
ΔLEMΔQRRR
Ab:GFP ratio
G
quantification of (G)
median antibody:GFP ratio
anti-IgG
WT
RA
ΔLEM
ΔQRRR
H
EMD mutant trafficking patterns
nucleo/cytoplasm lumen
no trafficking
trafficking
Cyb5 TM
ΔLEM
QRRR
LEM
TM
WT
ΔLEMΔQRRR
RA
AAAA
I
EMD protein stability by Western blot
WT
RA
ΔLEM
ΔLEMΔQRRR
Dox washout:
18hr
αGFP
αGAPDH
J
quantification of (I)
Fraction GFP remaining
WT
RA
ΔLEM
ΔLEMΔQRRR

Figure 2. Emerin's trafficking depends on its TMD, not on the LEM domain.

A) Surface anti-GFP antibody:GFP histogram of human WT EMD, ΔLEM, and EMD with mouse cytochrome B5 TMD ($EMD^{Cyb5\ TMD}$) chimera.

B) U2OS cells expressing mouse EMD-GFP and $EMD^{Cyb5\ TMD}$-GFP were induced with 1 ug/mL doxycycline for 24 hours, treated with 100nM lysosome blocking drug bafilomycin A1 (BafA1) overnight, and fixed and stained for lysosome marker Lamp1. Scale bars, 10 um.

C) TMD mutation strategy. The TM alpha helix of human EMD was divided into N-terminal and C-terminal halves, and the aromatic residues in each half were mutated to alanine to generate mutants with similar ΔG-insertion values. For the full TMD mutant, all aromatic residues were mutated to alanine, yielding a predicted ΔG-insertion of -2.299.

D) Surface antibody:GFP FACS histogram and **E)** quantification of the mutants diagramed in (C). *N* = 4 independent experiments

F) Surface antibody:GFP FACS histogram and **G)** quantification of mouse WT EMD, RA, ΔLEM, and ΔLEMΔQRRR truncation surface expression. *N* = 4 independent experiments.

H) Summary of emerin constructs that do or do not traffic.

I) Western blot analysis of emerin constructs induced with 2 ug/mL doxycycline for 48 hours, then washed and incubated for an 18 hour chase.

J) Quantification of Western blot band intensity from (I). GFP antibody signal after washout was divided by the respective unwashed condition to yield the fraction GFP remaining after doxycycline washout across 3 independent replicates.

For all panels: *** indicates adjusted P-value <0.0005, * indicates P = 0.0104. All P-values were obtained by one-way ANOVA with Šídák's or Tukey's multiple comparisons tests.

Figure 2 supplement

A *ΔG-insertion prediction of example tail-anchored TMDs*

protein	TM length	ΔG-ins	location
cyb5	17 aa	-0.23	ER
stx3	22 aa	-4.5	PM
emerin	23 aa	-4.05	INM/ER
lap2b	24 aa	-3.27	INM/ER

B *ΔG-transfer of single pass TMDs*

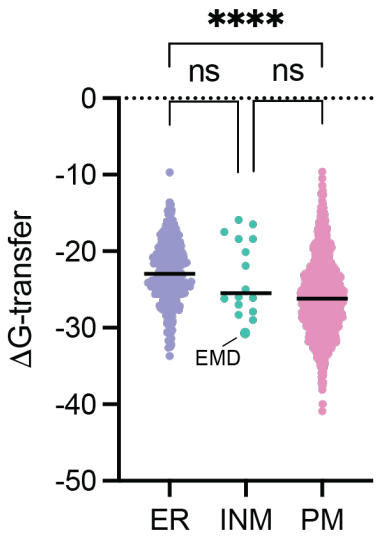

C *Lengths of single pass TMDs*

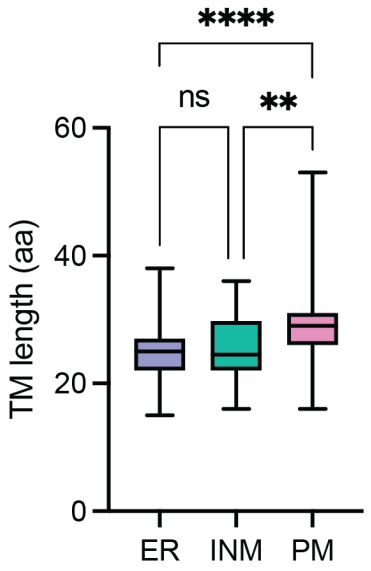

D *EMD LEM domain alignment*

```
xenopus        MENYKHMTDDELIETLQKCNITHGPIVGTTRTLYEKKLYEYERSKTR
d.rerio        MSSLSVKSDKEICQLLDEYGIKHGPIVESTRKLYEKKLNEAMAKKTK
r. macaque     MDDYADLSNTELTALLRRYNIPHGPVVGSTRRLYEQKIFEYETQRRR
human          MDNYADLSDTELTTLLRRYNIPHGPVVGSTRRLYEKKIFEYETQRRR
rat            MDDYAVLSDTELAAVLRQYNIPHGPILGSTRKLYEKKIFEYETQRRR
mouse          MDDYAVLSDTELAAVLRQYNIPHGPIVGSTRKLYEKKIFEYETQRRR
```

ΔLEM truncation

Figure 2 supplement: A) Lengths and predicted ΔG-insertion values of ER protein cytochrome B5, PM protein syntaxin 3, and emerin INM proteins emerin and Lap2β.
B) Single pass human transmembrane proteins from Membranome database plotted by free energy of transfer into a lipid bilayer. Lines represent median; **** indicates P < 0.0001 by one-way Anova with Tukey's multiple comparisons test.
C) Transmembrane domain length (by amino acid count) of the proteins in (B). ** indicates P = 0.0028; **** indicates P < 0.0001.
D) Protein sequence alignment of emerin's LEM domain across species. Conserved LEM domain amino acid class indicated in blue. QRRR motif is conserved in mammals and is exposed in the ΔLEM construct.

Figure 3

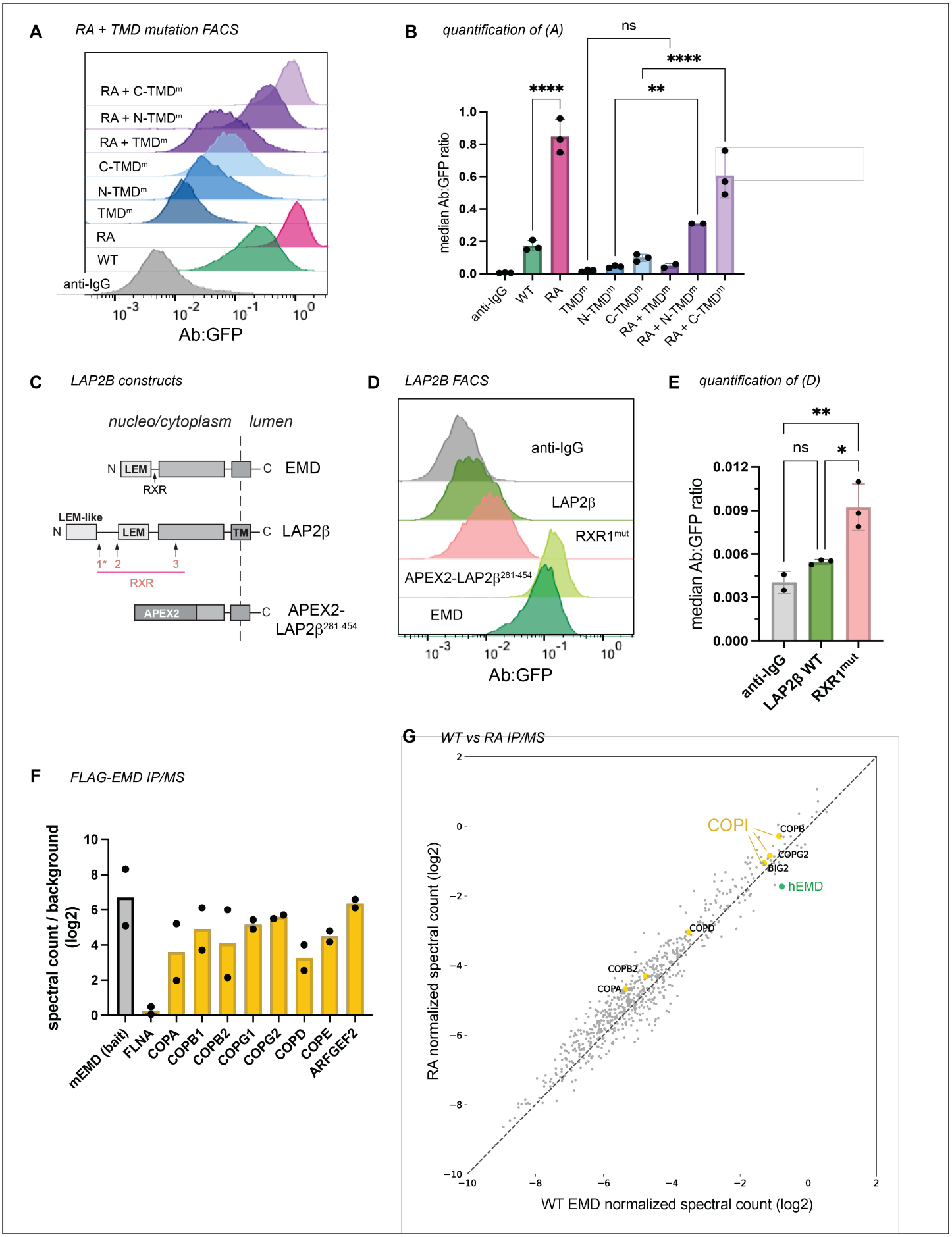
A
RA + TMD mutation FACS
RA + C-TMDm
RA + N-TMDm
RA + TMDm
C-TMDm
N-TMDm
TMDm
RA
WT
anti-IgG
Ab:GFP
B
quantification of (A)
ns
****
****
**
median Ab:GFP ratio
anti-IgG
WT
RA
TMDm
N-TMDm
C-TMDm
RA + TMDm
RA + N-TMDm
RA + C-TMDm
C
LAP2B constructs
nucleo/cytoplasm
lumen
N
LEM
RXR
C
EMD
LEM-like
LAP2β
TM
APEX2
APEX2-LAP2β281-454
D
LAP2B FACS
anti-IgG
LAP2β
RXR1mut
APEX2-LAP2β281-454
EMD
Ab:GFP
E
quantification of (D)
**
ns
*
median Ab:GFP ratio
anti-IgG
LAP2β WT
RXR1mut
F
FLAG-EMD IP/MS
spectral count / background (log2)
mEMD (bait)
FLNA
COPA
COPB1
COPB2
COPG1
COPG2
COPD
COPE
ARFGEF2
G
WT vs RA IP/MS
COPI
COPB
COPG2
BIG2
hEMD
COPD
COPB2
COPA
RA normalized spectral count (log2)
WT EMD normalized spectral count (log2)

Figure 3. RXR motif limits TMD-dependent trafficking of emerin and LAP2β without influencing COPI binding.
A) Surface anti-GFP:GFP histogram and **B)** quantification of indicated RA + TMD mutant combinations. ** indicates P = 0.0021. *N* = 3 independent experiments.
C) Diagram of LAP2β domain structure and position of RXR motifs. APEX2 fusion contains no RXR motifs.
D) Antibody:GFP histogram and **E)** quantification of the highest 25% GFP-expressing cells diagramed in (C). RXR^{mut} : LAP2β RXR1 mutated to AAA. * indicates P = 0.0173; ** indicates P = 0.0072
F) Spectral counts of COPI proteins immunoprecipitated by WT FLAG-EMD normalized to negative control IP. Spectral counts of the mouse EMD bait and common contaminant filamin A (FLNA) plotted for comparison. *N* = 2 independent experiments.
G) Spectral counts of proteins immunoprecipitated by FLAG-WT and FLAG-RA mouse EMD normalized to each respective bait. Dotted line represents equal co-immunoprecipitation with the two constructs. COPI proteins and endogenous human EMD highlighted in yellow and green, respectively.
All P-values were obtained by one-way ANOVA with Šídák's or Tukey's multiple comparisons tests.

Figure 3 supplement

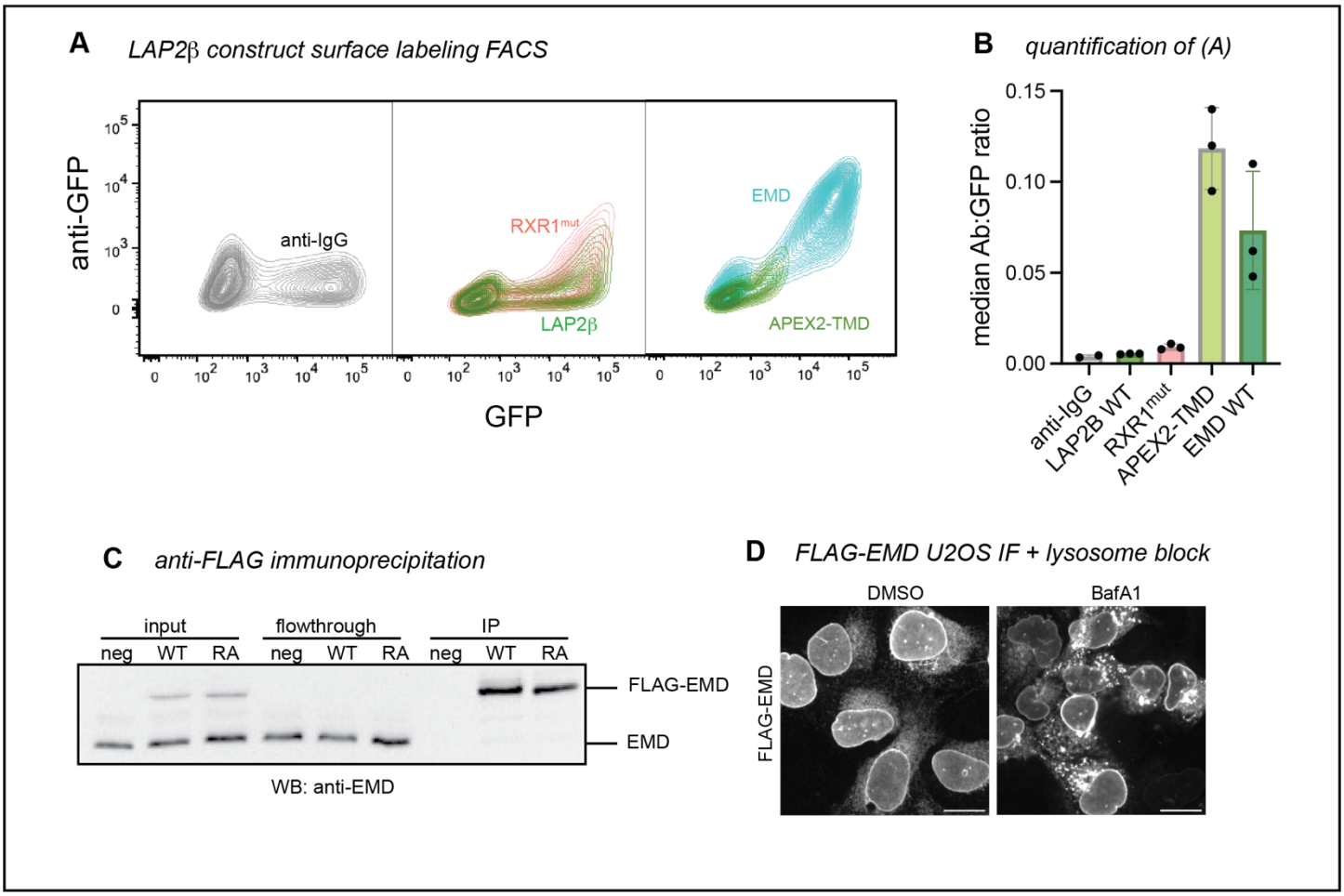

Figure 3 supplement: A) GFP versus surface anti-GFP FACS plots of negative control anti-IgG, WT LAP2β / RXR1mut, and WT EMD / LAP2β APEX2-TMD.
B) Median anti-GFP antibody:GFP ratio of the highest 25% GFP-expressing cells in (A).
C) Western blot analysis of anti-FLAG immunoprecipitations. U2OS cells expressing no FLAG construct (neg), FLAG-WT mouse EMD, and FLAG-RA mutant were lysed and incubated with anti-FLAG magnetic beads. Equal volume equivalents were separated by SDS-PAGE and blotted with an anti-EMD antibody to visualize tagged and untagged EMD.
D) U2OS cells expressing FLAG-EMD were incubated with lysosome blocker bafilomycin A1 (BafA1) overnight, then fixed and permeabilized with 0.1% Triton-X-100, 0.02% SDS, 10 mg/ml BSA in PBS. Cells were stained with anti-FLAG antibody to visualize relocalization during BafA1 treatment. Scale bars, 20 um.

Figure 4

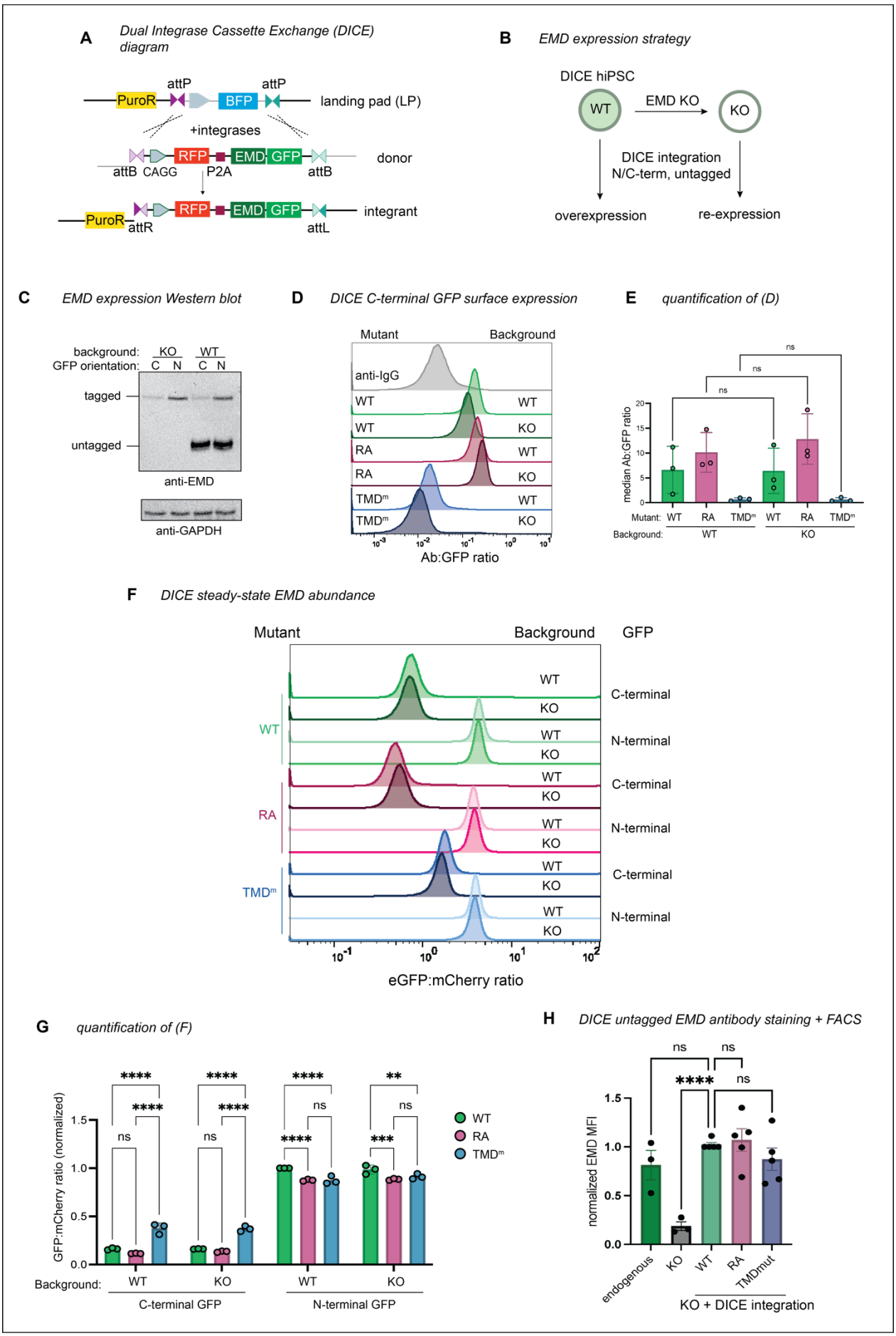

A
Dual Integrase Cassette Exchange (DICE) diagram
attP
attP
PuroR
BFP
landing pad (LP)
+integrases
RFP
EMD
GFP
donor
attB
CAGG
P2A
attB
PuroR
RFP
EMD
GFP
integrant
attR
attL
B
EMD expression strategy
DICE hiPSC
WT
EMD KO
KO
DICE integration
N/C-term, untagged
overexpression
re-expression
C
EMD expression Western blot
background:
KO
WT
GFP orientation:
C N
C N
tagged
untagged
anti-EMD
anti-GAPDH
D
DICE C-terminal GFP surface expression
Mutant
Background
anti-IgG
WT
WT
WT
KO
RA
WT
RA
KO
TMDm
WT
TMDm
KO
Ab:GFP ratio
E
quantification of (D)
ns
ns
ns
median Ab:GFP ratio
Mutant:
WT
RA
TMDm
WT
RA
TMDm
Background:
WT
KO
F
DICE steady-state EMD abundance
Mutant
Background
GFP
WT
KO
C-terminal
WT
KO
N-terminal
WT
KO
C-terminal
RA
WT
KO
N-terminal
WT
KO
C-terminal
TMDm
WT
KO
N-terminal
eGFP:mCherry ratio
G
quantification of (F)
GFP:mCherry ratio (normalized)
WT
RA
TMDm
Background:
WT
KO
WT
KO
C-terminal GFP
N-terminal GFP
H
DICE untagged EMD antibody staining + FACS
ns
ns
ns
normalized EMD MFI
endogenous
KO
WT
RA
TMDmut
KO + DICE integration

Figure 4. Safe harbor expression reveals that C-terminal GFP destabilizes emerin. **A)** Diagram of emerin integration into the AAVS1 locus. Landing pad BFP is exchanged for mCherry-P2A-emerin +/- GFP via Bxb1 and PhiC31 integrases. Integrases irreversibly recombine landing pad attP and donor attB sites into attR and attL sites.
B) Strategy to compare overexpressed emerin to knockout (KO) rescue.
C) Western blot analysis WT and EMD KO DICE hiPSCs expressing N- and C-terminally GFP-tagged emerin. Untagged endogenous EMD and GFP-tagged EMD are detected by the same anti-EMD antibody.
D) Anti-GFP surface labeling histogram and **E)** quantification of C-terminally tagged emerin integrants from (B-C). Statistical significance was determined using one-way ANOVA with Šídák's multiple comparisons test. *N* = 3 independent experiments.
F) FACS plot and **G)** quantification of steady state GFP abundance. Data were normalized to the GFP-EMD signal in the EMD WT background. *N* = 3 independent experiments. ** indicates P = 0.0079 by two-way ANOVA with Tukey's multiple comparisons test.
H) DICE landing pad WT, EMD KO, and KO re-integrated with untagged constructs were lifted, fixed, and stained with anti-EMD antibody. Fluorescence was quantified by flow cytometry and normalized to the WT DICE integrant. MFI, median fluorescence intensity of antibody signal. *N* = 5 replicates over 4 independent experiments. **** indicates P <0.0001 by mixed effects analysis.

Figure 4 supplement

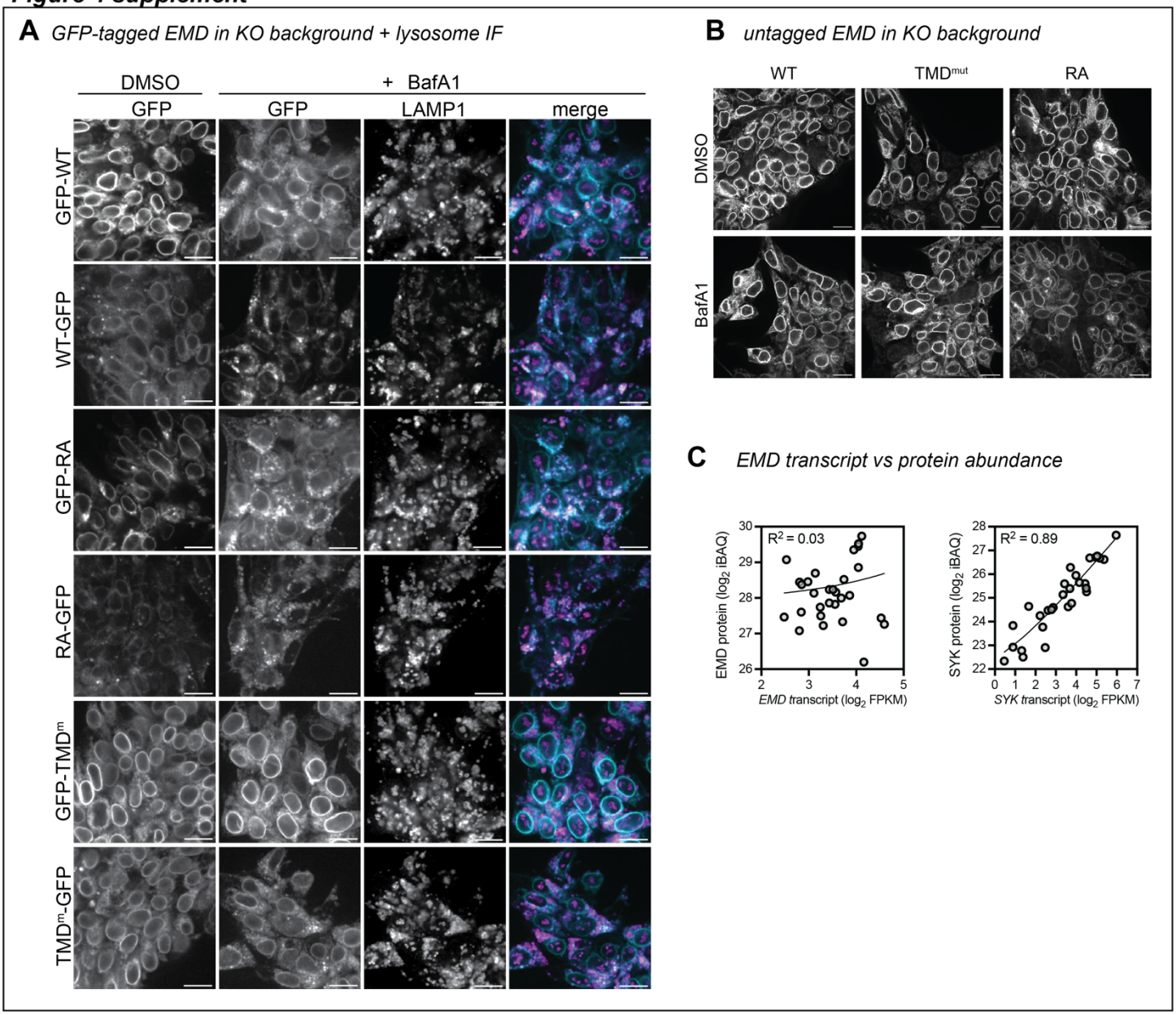

Figure 4 supplement: A) EMD KO DICE hiPSCs were integrated with GFP-tagged EMD constructs. Cells were treated with vehicle or lysosome blocker bafilomycin A1 (BafA1) overnight, then fixed and stained with anti-LAMP1 antibody.
B) EMD KO DICE hiPSCs were integrated with untagged EMD WT, TMD mutant, or RA mutant. Cells were treated overnight with BafA1, then fixed and stained with anti-EMD antibody. Scale bars, 20 um.
C) We mined a dataset of matched RNAseq and quantitative protein abundances across 29 human tissues to evaluate EMD transcript and protein abundances. EMD protein and transcript abundance are largely uncorrelated (R2 ~ 0), while, for comparison, the enzyme spleen tyrosine kinase (SYK) has well-correlated protein and RNA levels (R2 = 0.89)